Spectrochimica Acta Part A: Molecular and Biomolecular Spectroscopy 121 (2014) 404–414

Contents lists available at ScienceDirect

Spectrochimica Acta Part A: Molecular and Biomolecular Spectroscopy

journal homepage: www.elsevier.com/locate/saa

Spectroscopic (FT-IR, FT-Raman) investigations and quantum chemical calculations of 4-hydroxy-2-oxo-1,2-dihydroquinoline-7-carboxylic acid

Rajeev T. Ulahannan [a], C. Yohannan Panicker [b,*], Hema Tresa Varghese [c], C. Van Alsenoy [d], Robert Musiol [e], Josef Jampilek [f], P.L. Anto [g]

[a] Deparment of Physics, Mar Ivanios College, Trivandrum, Kerala, India
[b] Department of Physics, TKM College of Arts and Science, Kollam, Kerala, India
[c] Department of Physics, Fatima Mata National College, Kollam, Kerala, India
[d] Department of Chemistry, University of Antwerp, B2610 Antwerp, Belgium
[e] Institute of Chemistry, University of Silesia, Szkolna 9, 40007 Katowice, Poland
[f] Department of Chemical Drugs, Faculty of Pharmacy, University of Veterinary and Pharmaceutical Sciences, Palackeho 1/3, 61242 Brno, Czech Republic
[g] Department of Physics, Christ College, Irinjalakkuda, Thrissur, Kerala, India

HIGHLIGHTS

- IR, Raman, NBO analysis and MEP were reported.
- The wavenumbers are calculated theoretically using Gaussian09 software.
- The wavenumbers are assigned using PED analysis.
- The geometrical parameters are in agreement with the reported literature.

GRAPHICAL ABSTRACT

In this work, the vibrational spectral analysis was carried out using FT-IR and FT-Raman spectroscopy for 4-hydroxy-2-oxo-1,2-dihydroquinoline-7-carboxylic acid. The computations were performed at HF and DFT levels of theory to get the optimized geometry and vibrational wavenumbers of the normal modes of the title compound. The complete vibrational assignments of wavenumbers were made on the basis of potential energy distribution and using Gaussview software. The calculated HOMO and LUMO energies show the chemical activity of the molecule. The stability of the molecule arising from hyper-conjugative interaction and charge delocalization has been analyzed using NBO analysis. The calculated geometrical parameters are in agreement with that of similar derivatives. The stability of the molecule arising from hyper-conjugative interaction and charge delocalization has been analyzed using NBO analysis.

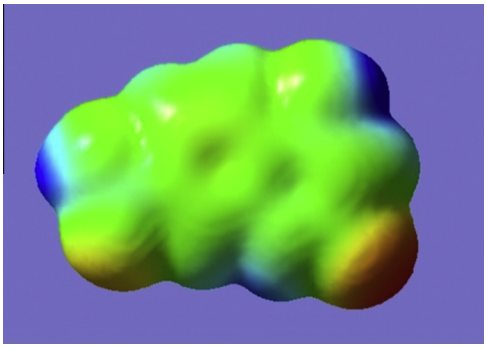

ARTICLE INFO

Article history:
Received 31 August 2013
Received in revised form 22 October 2013
Accepted 31 October 2013
Available online 9 November 2013

Keywords:
FTIR

ABSTRACT

Quinoline derivatives have good nonlinear optical properties and have been extensively studied due to their great potential application in the field of organic light emitting diodes. Quantum chemical calculations of the equilibrium geometry, harmonic vibrational frequencies, infrared intensities and Raman activities of 4-hydroxy-2-oxo-1,2-dihydroquinoline-7-carboxylic acid in the ground state were reported. Potential energy distribution of normal modes of vibrations was done using GAR2PED program. The synthesis, ^{1}H NMR and PES scan results are also discussed. Nonlinear optical behavior of the examined molecule was investigated by the determination of first hyperpolarizability. The calculated HOMO and LUMO energies show the chemical activity of the molecule. The stability of the molecule arising from

* Corresponding author. Tel.: +91 9895370968.
E-mail address: cyphyp@rediffmail.com (C.Y. Panicker).

http://dx.doi.org/10.1016/j.saa.2013.10.114

FT-Raman
Quinoline
PED
MEP

hyperconjugative interaction and charge delocalization has been analyzed using NBO analysis. The calculated geometrical parameters are in agreement with that of similar derivatives.

Introduction

Quinoline derivatives possess non-centro symmetry and hence they are used in the synthesis of molecules having non-linear responses [1,2]. Some quinoline derivatives have good nonlinear optical properties [3,4] and have been extensively studied due to their great potential application in the field of organic light emitting diodes (OLED) [5–16]. Quinolines have good electron mobility, good thermal and oxidative stabilities, high photoluminescence efficiency and good film forming properties which is important for their use in OLEDs [17,18]. Certain derivatives extracted from the plant *Camptotheca acuminata* have been a potential anticancer drug. Its inhibition completely blocks the cell proliferation and hence the cancer growth and has shown their anticancer activity against a wide spectrum of human malignancies, including, lung, prostrate, breast, colon, stomach, ovaries, carcinomas, melanoma, lymphomas and sarcomas [19–21]. Quinoline derivatives are well known for its anti-malarial, antifungal and anti-amoebic activities [22]. In addition to the medical applications, these derivatives can function as, pesticides, corrosion inhibitors and components in photographic, digital recording devices and fabric dyes [23]. In the present work, IR and Raman spectra of the title compound are reported both experimentally and theoretically. Also the NBO analysis, molecular electrostatic potential, NMR studies and first hyperpolarizability is also reported.

Experimental details

The synthesis of the quinoline derivative was done by [24] adding corresponding anilines (0.20 ml) and malonic acid (0.18 mol). Naphthalene (0.12 mol) and malonic acid (0.18 mol) were melted under stirring at temperature control (<150 °C) to avoid decarboxylation of the acid. $POCl_3$ (0.36 mol) was then added dropwise over 30 min and aminosalicylic acid (0.1 mol) was then added. The resulting mixture was heated for 30 min and allowed to cool. Water (100 ml) was added to the warm mixture and the solution was alkalized with 20% NaOH to pH 9. After cooling on ice precipitated naphthalene, it was filtered and the filtrate was acidified to pH 2. The product was filtered again and crystallized from acetic acid.

The FT-IR spectrum (Fig. 1) was recorded using KBr pellets on a DR/Jasco FT-IR 6300 spectrometer. The FT-Raman spectrum (Fig. 2) was obtained on a Bruker RFS 100/s, Germany. For excitation of the spectrum the emission of Nd:YAG laser was used, excitation wavelength 1064 nm, maximal power 150 mW, measurement on solid sample. ^1H NMR spectra was recorded on a Bruker AM-500 (500 MHz for ^1H), Bruker BioSpin Corp., Germany. Chemicals shifts are reported in ppm (δ) to internal Si $(CH_3)_4$, when diffused easily exchangeable signals are omitted.

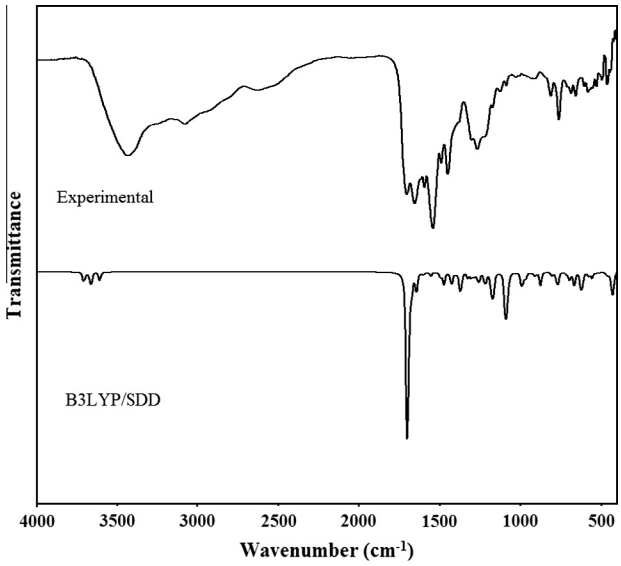

Fig. 1. FT-IR spectrum of 4-hydroxy-2-oxo-1,2-dihydroquinoline-7-carboxylic acid.

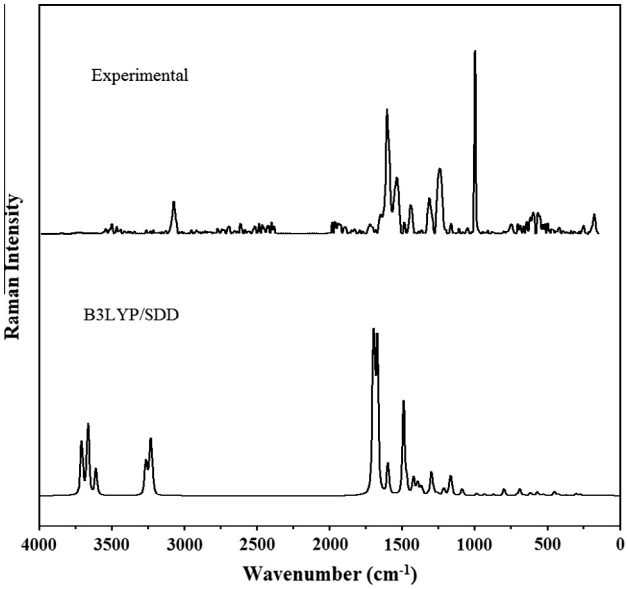

Fig. 2. FT-Raman spectrum of 4-hydroxy-2-oxo-1,2-dihydroquinoline-7-carboxylic acid.

Computational details

Calculations of the title compound are carried out with Gaussian09 program [25] using the HF/6-31G*, B3LYP/6-31G* and B3LYP/SDD quantum chemical calculation methods to predict the molecular structure and vibrational wave numbers. Molecular geometry was fully optimized by Berny's optimization algorithm using redundant internal coordinates. Harmonic vibrational wave numbers are calculated using the analytic second derivatives to confirm the convergence to minima on the potential surface. The wave number values computed at the Hartree–Fock level contain known systematic errors due to the negligence of electron correlation. We therefore, have used the scaling factor value of 0.8929 for HF method. The DFT hybrid B3LYP functional and SDD methods tend to overestimate the fundamental modes, therefore scaling factor of 0.9613 has to be used for obtaining a considerably better agreement with experimental data [26]. The Stuttgart/Dresden effective core potential basis set (SDD) was chosen particularly

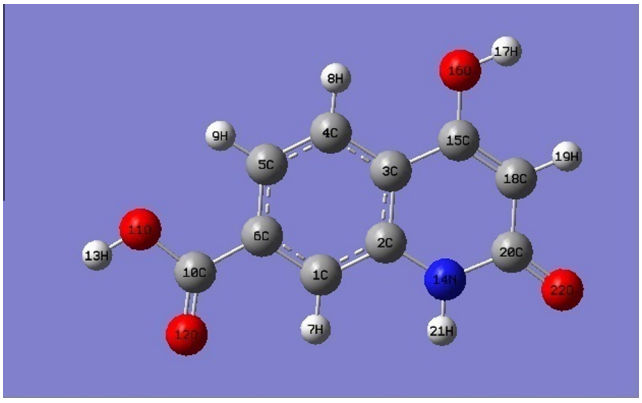

Fig. 3. Optimized geometry (SDD) of 4-hydroxy-2-oxo-1,2-dihydroquinoline-7-carboxylic acid.

because of its advantage of doing faster calculations with relatively better accuracy and structures [27,28]. Then frequency calculations were employed to confirm the structure as minimum points in energy. Parameters corresponding to optimized geometry (SDD) of the title compound (Fig. 3) are given in Table 1. The absence of imaginary wavenumbers on the calculated vibrational spectrum confirms that the structure deduced corresponds to minimum energy. The assignments of the calculated wave numbers are aided by the animation option of GAUSSVIEW program, which gives a visual presentation of the vibrational modes [29]. The potential energy distribution (PED) is calculated with the help of GAR2PED software package [30].

Results and discussion

IR and Raman spectra

The observed IR and Raman bands and calculated (scaled) wavenumbers and assignments are given in Table 2. The NH stretching vibrations give rise to bands at 3500–3300 cm^{-1} [31,32]. In the present study the bands observed at 3430 cm^{-1} in

Table 1
Optimized geometrical parameters (B3LYP/SDD) of 4-hydroxy-2-oxo-1,2-dihydroquinoline-7-carboxylic acid, atom labeling according to Fig. 3.

Bond lengths (Å)		Bond angles (°)		Dihedral angles (°)	
C1—C2	1.4020	C2—C1—C6	120.3	C6—C1—C2—C3	−0.8
C1—C6	1.3915	C2—C1—H7	120.8	C6—C1—C2—N14	179.3
C1—H7	1.0856	C6—C1—H7	118.9	H7—C1—C2—C3	179.0
C2—C3	1.4171	C1—C2—C3	119.6	H7—C1—C2—N14	−0.8
C2—N14	1.3771	C1—C2—N14	121.3	C2—C1—C6—C5	1.4
C3—C4	1.4043	C3—C2—N14	119.1	C2—C1—C6—C10	−179.0
C4—C5	1.3860	C2—C3—C4	119.4	H7—C1—C6—C5	−178.6
C4—H8	1.0841	C2—C3—C15	117.5	H7—C1—C6—C10	0.2
C5—C6	1.4092	C4—C3—C15	123.1	C1—C2—C3—C4	0.3
C5—H9	1.0868	C3—C4—C5	120.7	C1—C2—C3—C15	−179.9
C6—C10	1.5024	C3—C4—H8	118.8	N14—C2—C3—C4	179.6
C10—O11	1.3595	C5—C4—H8	120.6	N14—C2—C3—C15	0.1
C10—O12	1.2078	C4—C5—C6	119.9	C1—C2—N14—C20	179.9
O11—H13	0.9710	C6—C5—H9	121.0	C1—C2—N14—H21	0.2
N14—C20	1.4033	C1—C6—C5	120.1	C3—C2—N14—C20	−0.1
N14—H21	1.0135	C1—C6—C10	117.0	C3—C2—N14—H21	−179.8
C15—O16	1.3570	C5—C6—C10	122.9	C2—C3—C4—C5	0.8
C15—C18	1.3608	C6—C10—O11	116.6	C2—C3—C4—H8	−178.7
O16—H17	0.9710	C4—C5—H9	119.0	C15—C3—C4—C5	−179.7
C18—H19	1.0857	C6—C10—O12	123.3	C15—C3—C4—H8	0.8
C18—C20	1.4561	O11—C10—O12	120.1	C2—C3—C15—O16	180.0
C20—O22	1.2245	C10—O11—H13	110.2	C2—C3—C15—C18	0.2
		C2—N14—C20	125.8	C4—C3—C15—O16	0.4
		C2—N14—H21	119.6	C4—C3—C15—C18	−179.6
		C20—N14—H21	114.6	C3—C4—C5—C6	0.3
		C3—C15—O16	114.8	H8—C4—C5—H9	2.2
		C3—C15—C18	121.3	H9—C5—C6—C1	176.1
		O16—C15—C18	123.9	H9—C5—C6—C10	−2.6
		C15—O16—H17	109.2	C1—C6—C10—O11	−19.9
		C15—C18—H19	121.9	C4—C5—C6—C1	0.9
		C15—C18—C20	122.2	C4—C5—C6—C10	−179.6
		H19—C18—C20	116.0	C3—C4—C5—H9	177.3
		N14—C20—C18	114.2	H8—C4—C5—C6	179.3
		N14—C20—O22	120.4	C1—C6—C10—O12	−20.6
		C18—C20—O22	125.4	C5—C6—C10—O11	−22.0
				C5—C6—C10—O12	158.1
				C6—C10—O11—H13	9.8
				O12—C10—O11—H13	170.1
				C2—N14—C20—C18	0.1
				H21—N14—C20—C18	179.7
				H21—N14—C20—O22	0.2
				C3—C15—O16—H17	−179.7
				C18—C15—O16—H17	0.3
				C3—C15—C18—H19	−180.0
				C3—C15—C18—C20	0.6
				O16—C15—C18—H19	−0.0
				O16—C15—C18—C20	−180.0
				C15—C18—C20—N14	−0.0
				C15—C18—C20—O22	180.0
				H19—C18—C20—N14	180.0
				H19—C18—C20—O22	−0.0

Table 2
IR, Raman bands and calculated (scaled) wavenumbers of 4-hydroxy-2-oxo-1,2-dihydroquinoline-7-carboxylic acid and assignments.

HF/6-31g*			B3LYP/6-31g*			B3LYP/SDD			IR	Raman	Assignments
υ(cm^{-1})	IR_I	R_A	υ(cm^{-1})	IR_I	R_A	υ(cm^{-1})	IR_I	R_A	υ(cm^{-1})	υ(cm^{-1})	
3618	80.95	40.08	3528	48.78	179.30	3563	62.94	167.01	–	–	υOH(100)
3602	109.34	119.50	3508	18.35	61.88	3522	81.93	212.34	–	3544	υOH(100)
3444	72.13	53.68	3471	44.24	74.98	3468	49.18	72.69	3430	3469	υNH(100)
3056	1.14	96.51	3126	1.24	94.67	3138	0.43	110.60	–	3126	υCH(97)
3043	2.55	110.31	3110	2.74	121.22	3117	0.35	40.22	–	–	υCH(99)
3034	1.09	44.23	3102	1.60	46.23	3106	3.22	107.44	–	–	$\upsilon C_{18}H_{19}$(99)
3015	8.72	83.19	3080	10.97	84.28	3094	1.70	38.44	3077	3077	υCH(97)
1731	350.63	80.70	1690	225.37	131.99	1634	649.05	203.79	1651	1652	$\upsilon C_{10}O_{12}$(80)
1684	1149.55	97.33	1661	703.11	118.11	1627	355.43	257.45	1610	1609	$\upsilon C_{20}O_{22}$(62)
1645	8.24	189.26	1616	10.55	313.93	1607	90.23	367.51	1610	1609	$\upsilon C_{15}C_{18}$(56), υPh(24)
1621	61.88	39.01	1596	48.37	13.97	1578	90.04	4.21	1590	–	υPh(65), $\upsilon C_{15}C_{18}$(16)
1567	19.40	36.01	1544	11.72	51.37	1535	11.73	88.25	1540	1537	υPh(64), $\upsilon C_{15}C_{18}$(11)
1519	8.86	1.88	1508	21.33	0.87	1491	18.80	0.78	1486	1488	υPh(60), υRing(11)
1460	9.38	119.02	1449	18.20	167.87	1433	24.50	214.07	1445	1445	υPh(57), δNH(18)
1428	83.02	25.56	1431	51.98	11.17	1412	63.39	34.35	–	1409	$\delta C_{18}H_{19}$(13), $\delta O_{16}H_{17}$(60)
1380	62.3	1.08	1370	61.34	11.68	1368	75.85	52.08	1376	1366	δNH(44), υPh(41)
1316	180.70	111.57	1352	15.84	80.40	1340	11.40	42.18	–	–	υPh(59), δCH(20)
1304	17.21	9.99	1287	3.63	11.83	1313	129.69	27.06	1298	1319	$\delta O_{11}H_{13}$(22), $\upsilon C_{10}O_{11}$(51), υC_6C_{10}(16)
1272	25.84	34.34	1271	116.30	25.19	1270	30.07	4.03	1262	–	υCN(44), δOH(48)
1241	243.90	4.50	1252	52.41	50.30	1247	31.81	63.88	–	1240	δCH(48), υRing(24)
1225	285.54	28.09	1216	84.76	11.02	1230	17.42	7.02	–	1202	υCN(64), $\delta O_{16}H_{17}$(15)
1205	42.48	8.28	1206	395.46	53.42	1206	69.70	6.95	1214	–	$\upsilon C_{15}O_{16}$(62), $\delta C_{18}H_{19}$(21)
1182	48.27	13.20	1191	88.29	8.43	1167	77.16	22.57	1163	1166	$\delta O_{16}H_{17}$(35), $\delta C_{18}H_{19}$(48)
1143	173.59	10.20	1156	83.06	30.77	1130	60.72	7.88	–	–	δCH(69), $\delta O_{11}H_{13}$(15), υC_6C_{10}(14)
1132	138.87	2.37	1137	77.83	7.76	1120	164.53	64.12	1118	1113	δCH(64), υPh(19)
1091	48.14	1.08	1075	82.98	2.09	1045	235.06	17.15	–	1051	υCC(47), δCH(20), δPh(12)
1056	56.34	4.06	1051	72.18	3.29	1035	141.22	2.71	1020	1022	υCC(47),υPh(17), $\upsilon C_{15}O_{16}$(15)
1039	1.47	1.18	966	7.66	1.27	1002	0.02	0.05	997	–	υCC(53), υPh(21), $\upsilon C_{15}O_{16}$(13)
967	50.86	2.17	959	56.82	2.82	947	99.07	7.39	–	947	γCH(88)
965	62.06	1.84	912	11.53	2.45	926	37.90	0.14	–	913	δPh(29), γOH(45)
913	3.99	4.00	908	27.14	3.05	897	3.41	5.23	900	885	γCH(76), τPh(10)
880	30.01	1.69	836	85.94	2.87	869	27.26	1.05	–	–	γCH(55), $\gamma C_{18}H_{19}$(31)
868	136.98	5.88	829	0.46	0.94	836	66.74	4.04	804	–	$\gamma C_{18}H_{19}$(44), γCH(20), τRing(12)
790	50.89	2.89	779	9.53	12.75	769	17.40	0.47	–	788	δRing(26), υPh(55)
785	14.12	9.40	758	16.44	2.53	766	1.52	18.04	755	752	τPh(13), $\delta C_{10}O_{12}$(53), γCC(14)
782	97.86	3.30	751	86.04	0.71	735	93.02	0.20	–	726	τPh(26), γNH(54)
739	28.01	2.59	714	14.59	2.49	719	0.21	1.08	703	706	$\gamma C_{10}O_{12}$(43), δPh(10), $\delta C_{10}O_{11}$(10)
707	11.93	1.47	701	7.16	1.59	679	12.52	4.22	676	696	$\gamma C_{20}O_{22}$(48), τRing(27)
682	12.40	10.55	677	11.67	13.81	662	36.55	15.42	651	665	δPh(40), δRing(30)
648	39.32	6.77	639	40.63	4.05	636	66.28	1.35	–	–	$\gamma O_{16}H_{17}$(46), τPh(28)
634	10.50	3.47	620	5.30	3.21	626	0.17	0.41	–	621	$\delta C_{20}O_{22}$(23), δPh(22), $\delta C_{15}O_{16}$(41)
608	4.02	1.23	601	2.33	0.96	592	116.41	8.75	597	–	γNH(32), δPh(37), δRing(15)
580	10.13	1.41	570	3.42	2.37	582	17.98	1.11	560	571	δPh(25), $\delta C_{10}O_{11}$(32), τRing(12), τCC_{15}(18)
555	7.69	4.41	551	3.20	4.59	548	19.21	8.44	548	553	τPh(14), τRing(28), δCC(25)
514	2.54	4.60	511	3.06	4.38	528	28.78	1.71	519	500	δRing(50), $\tau O_{11}H_{13}$(17)
489	10.04	0.63	484	13.89	1.00	504	5.79	4.91	488	–	$\tau O_{11}H_{13}$(57), δCN(26)
449	22.45	4.02	467	75.22	2.39	476	1.96	0.50	457	476	τPh(25), $\delta C_{10}O_{11}$(35), τRing(18)
439	35.26	1.45	449	132.0	3.41	440	8.16	1.53	439	446	$\tau O_{16}H_{17}$(46), τPh(21), τRing(12)
414	296.01	4.96	438	52.57	9.11	435	12.03	10.34	–	422	δRing(61), δPh(18)
403	21.33	3.02	412	31.77	3.33	407	151.85	4.93	415	396	τPh(44), $\tau O_{16}H_{17}$(21), γCC(10), τRing(10)
363	53.38	1.69	362	29.43	1.94	355	29.78	1.80	–	358	$\delta C_{15}O_{16}$(29), δRing(38), δPh(19)
303	27.37	2.98	302	15.22	4.31	292	4.63	6.00	–	–	$\delta C_{10}O_{11}$(46), δRing(15)
287	7.75	3.06	282	7.22	2.98	285	13.99	0.56	–	285	τRing(42), τPh(26), γNH(11)
264	4.84	3.07	264	3.71	3.77	259	1.35	3.51	–	252	δPh(50), $\delta C_{15}O_{16}$(29)
223	11.23	0.87	222	9.30	0.52	225	0.01	0.73	–	216	τRing(64), γNH(11)
202	0.42	1.23	197	0.21	1.38	194	0.67	1.54	–	179	τRing(57), γNH(16)
143	8.20	11.40	144	6.91	1.37	139	0.63	1.10	–	–	δRing(66)
111	4.12	1.02	110	3.66	1.04	111	2.65	0.67	–	–	τRing(59), γNH(22)
78	4.02	1.49	78	2.77	1.74	80	0.02	0.75	–	–	τRing(59), γNH(12), $\tau C_{10}O_{11}$(11)
59	4.47	1.19	54	4.00	1.18	56	0.37	0.21	–	–	τPh(24), τRing(60), γNH(10)

υ-stretching; δ-in-plane deformation; γ-out-of-plane deformation; τ-twisting; Ph-Phenyl ring; Ring-quinoline ring; In the assignment column the potential energy distributions are given in brackets.

IR, 3469 cm^{-1} in Raman and 3468 cm^{-1} (SDD) are assigned as NH stretching vibrations. N—H group show bands at 1510–1500, 1350–1250 and 740–730 cm^{-1} [33]. According to literature, if N—H is a part of a closed ring [32,33] the C—N—H deformation band is absent in the region 1510–1500 cm^{-1}. For the title compound the C—N—H deformation band is observed at 1366 cm^{-1} in the Raman spectrum, 1376 cm^{-1} in the IR spectrum and at 1368 cm^{-1} theoretically. The out of plane NH deformation is expected in the region 650 ± 50 cm^{-1} [34] and bands at 726 cm^{-1} in Raman and 735 cm^{-1} in SDD are assigned as this mode. Minitha et al. [35] reports υNH at 3469 cm^{-1}, δNH at 1300 cm^{-1} and γNH at 535 cm^{-1}. Panicker et al. reported the out-of-plane bending mode of NH at 746 cm^{-1}, theoretically [36]. The CN stretching modes are expected [37] in the range 1100–1300 cm^{-1}. The bands observed at

1262 cm^{-1} in IR, 1202 cm^{-1} in Raman and at 1270, 1230 cm^{-1} theoretically (SDD) are assigned as CN stretching modes. Panicker et.al reported the CN stretching mode at 1215 cm^{-1} theoretically [36].

According to Socrates [33] the C=C stretching is expected around 1600 cm^{-1} when conjugated with C=O. The C_{20}=O_{22} and C_{15}=C_{18} stretching bands are assigned at 1627 (SDD), 1610 cm^{-1} (IR), 1609 cm^{-1} (Raman) and at 1607 cm^{-1} (SDD), 1610 cm^{-1} (IR), 1609 cm^{-1} (Raman), respectively. The deformation bands of C=O and C=C are also identified and assigned (Table 2).

The carboxylic group is characterized by the OH stretch, C=O stretch and OH out-of-plane deformation and even by the C—O stretch and OH in-plane deformation. The C=O stretching vibration in the spectra of carboxylic acids give rise to a strong band in the region 1600–1700 cm^{-1} [34]. The band observed at 1651 cm^{-1} in the IR spectrum1652 cm^{-1} in the Raman spectrum and at 1634 cm^{-1} (SDD) is assigned as C=O stretching mode. The OH in-plane deformation, coupled to the C—O stretching mode is expected in the region 1390 ± 55 cm^{-1} [34], and the band at 1262 cm^{-1} (IR), 1270 cm^{-1} (SDD) is assigned as the in-plane bending of OH group which is not pure but contains contributions from other modes also. The C(=O)O stretching mode coupled to OH in-plane bending exhibits a band in the region 1250 ± 80 cm^{-1} and the SDD calculation give C—O stretching mode at 1313 cm^{-1}. Experimentally bands are observed at 1298 cm^{-1} in the IR spectrum and at 1319 cm^{-1} in the Raman spectrum. The deformation bands, out-of-plane OH, in-plane C=O and out-of-plane C=O are expected in the regions, 905 ± 65, 725 ± 95 and 595 ± 85 cm^{-1}, respectively [34]. These bands are assigned at 913 cm^{-1} (Raman), 926 (SDD), and 755 (IR), 752 (Raman), 766 cm^{-1} (SDD) and 703 (IR), 706 (Raman), 719 cm^{-1} (SDD) respectively. The —C(=O)O rocking mode is expected in the region 445 ± 120 cm^{-1} [34], and in the present case the SDD calculations give this mode at 476 cm^{-1}. Varghese et al., [38] reported COOH deformation bands at 785 cm^{-1} and 378 cm^{-1}.

For the hydroxyl group, the OH group provides three normal vibrations; the stretching vibration OH, in-plane and out-of-plane deformations δOH and γOH. The in-plane OH deformation [34] is expected in the region1440 ± 40 cm^{-1} and the band at 1409 in Raman spectrum and at 1412 cm^{-1} (SDD) is assigned as this mode. The stretching of hydroxyl group C—O appears at 1214 cm^{-1} in the IR spectrum and the calculated value is 1206 cm^{-1} (SDD) and this band is not pure, but contains significant contributions from other modes also. This band is expected in the region 1220 ± 40 cm^{-1} [39–41]. The out-of-plane deformation is expected generally in the region 650 ± 80 cm^{-1} [34] and in the present case it is assigned at 636 cm^{-1} theoretically (SDD). For paracetamol, the C—O stretching mode and out-of-plane OH are reported at 1240 and 620 cm^{-1}, respectively [42]. The SDD calculations give OH stretching at 3563 cm^{-1}.

Aromatic compounds commonly exhibit multiple weak bands in the region 3100–3000 cm^{-1}, due to aromatic CH stretching vibrations [34]. However, these bands are rarely useful because they overlap with one another resulting in stronger absorption in this region. The SDD calculations give the CH stretching modes of the phenyl ring at 3138, 3117, 3094 cm^{-1}. The bands observed at 3077 cm^{-1} in the IR spectrum and at 3126, 3077 cm^{-1} in the Raman spectrum are assigned as CH stretching modes of the phenyl ring. For the title compound, the bands at 1118 (IR), 1113, 1240 (Raman) and 1120, 1130, 1247 cm^{-1} (SDD) are assigned as the CH in-plane bending modes of the phenyl ring. The CH out-of-plane deformations are expected below 1000 cm^{-1} [34] and for the title compound, the SDD calculations give bands at 947, 897 and 869 cm^{-1} as γCH modes. Experimentally bands are observed at 900 cm^{-1} in the IR spectrum and at 947, 885 cm^{-1} in the Raman spectrum.

The benzene ring possesses six ring stretching modes of which the four with the highest wavenumbers occurring near 1600, 1580, 1490 and 1440 cm^{-1} are good group vibrations [34]. The bands observed at 1590, 1540, 1486, 1445, 1376 cm^{-1} in the IR spectrum, 1537, 1488, 1445, 1366 cm^{-1} in the Raman spectrum and at 1578, 1535, 1491, 1433, 1368, 1340 cm^{-1} theoretically (SDD) are assigned as phenyl ring stretching modes. These modes are expected in the region 1250–1620 cm^{-1} [34]. In the case of tri-substituted benzenes, with mixed substituent, the ring breathing mode is expected in the range 600–750 cm^{-1} [40] and in the present case, the band observed at 788 cm^{-1} in the Raman spectrum and at 769 cm^{-1} (SDD) is assigned as the ring breathing mode of the phenyl ring. Mary et al., [43] reported the ring breathing mode of the tri-substituted benzene ring at 738 cm^{-1}.

In the present case, the quinoline ring modes are observed at 1610, 1445, 1020 (CC stretching modes), 1262 (CN stretch) in IR, 1609, 1051, 1022 (CC stretching modes), 1202 (CN stretch) in Raman, 1607, 1433, 1045, 1035 (CC stretching modes), 1270, 1230 cm^{-1} (CN stretch) theoretically (SDD). For the title compound, the in-plane vibrations of the quinoline ring are observed at 519 cm^{-1} in IR, 500, 422 cm^{-1} in Raman and 528, 435 cm^{-1} in SDD. The torsional modes are seen at 285, 216 cm^{-1}, in Raman and 285, 225 cm^{-1} in SDD. The other deformations modes of the phenyl and quinoline ring are also identified and assigned (Table 2). The in plane bending of quinoline ring is reported by Chowdhury et al. [44] at 526, 472, 508, 624, 829, 869 cm^{-1} and the ring vibrations at 1245, 1383, 1434, 1470, 1593, 1621 cm^{-1} in the Raman spectrum and 760 cm^{-1} as the ring breathing mode. Krishnakumar et al. reported the out of plane bending of quinoline derivatives at 586, 601, 634, 505, 538, 612 cm^{-1} theoretically [45]. The substituent sensitive modes of the rings are also identified and assigned (Table 2).

Optimized geometrical parameters

To best of our knowledge, no X-ray crystallographic data of the title compound have yet been reported. However, the theoretical results (SDD) obtained are almost comparable with the reported structural parameters of similar derivates. For the title compound the bond length of C_5—C_6 is observed as 1.4092 Å and this length is greater than that of C_4—C_5 (1.3860 Å) because of the delocalisation of electron density of C_5—C_6 due to the presence of C=O group. The C_{15}=C_{18} could be assumed a double bond character due to the lesser bond length 1.3608 Å. The greater bond length of C_1—C_2 (1.4020 Å) is due to delocalisation of electron density due to the adjacent quinoline ring. It has been reported that the bond lengths of C_1—C_2 is 1.4188 Å, C_5—C_6 is 1.415 Å and C_{15}=C_{18} is 1.3679 Å [46]. The bond angle C_1—C_2—C_3 (119.6°) and C_2—C_3—C_4 (119.4°) is lesser than 120° because of the presence of quinoline ring. The angles C_2—N_{14}—C_{20} and C_3—C_{15}—C_{18} are 125.8 and 121.3° respectively, which can be assumed as due to the presence of OH group which is electropositive. The presence of higher electronegative group C=O would be the reason for the greater bond angle of N_{14}—C_{20}—C_{18} (114.2°). Yurdakul and Yurdakul reported the bond angles as C_1—C_2—C_3 (118.9), C_2—C_3—C_4 (119.3), C_2—N_{14}—C_{20} (118.93), C_3—C_{15}—C_{18} (119.85), N_{14}—C_{20}—C_{18} (122.82) [46]. The C_{10}=O_{12} group is slightly tilted from the tri-substituted phenyl ring as evident from the dihedral angle C_1—C_6—C_{10}—O_{11} = −19.9°.

HOMO and LUMO

HOMO (Highest Occupied Molecular Orbital) and LUMO (Lowest Unoccupied Molecular Orbital) are the very important parameters for quantum chemistry. The conjugated molecules are characterized by a HOMO–LUMO separation, which is the result of a significant degree of ICT (Intra-molecular Charge Transfer) from the end-capping electron-donor groups to the efficient electron-acceptor groups through π-conjugated path. The strong

charge transfer interaction through π-conjugated bridge results in substantial ground state donor–acceptor mixing and the appearance of a charge transfer band in the electronic absorption spectrum. The atomic orbital components of the frontier molecular orbitals are shown in Figs. 4 and 5. The HOMO–LUMO gap is found to be 3.073 eV.

Molecular electrostatic potential (MEP)

MEP is related to the ED and is a very useful descriptor in understanding sites for electrophilic and nucleophilic reactions as well as hydrogen bonding interactions [47,48]. The electrostatic potential $V(r)$ is also well suited for analyzing processes based on the "recognition" of one molecule by another, as in drug-receptor, and enzyme–substrate interactions, because it is through their potentials that the two species first "see" each other [49,50]. To predict reactive sites of electrophilic and nucleophilic attacks for the investigated molecule, MEP at the B3LYP/6-31G(d,p) optimized geometry was calculated. The negative (red and yellow) regions of MEP were related to electrophilic reactivity and the positive (blue) regions to nucleophilic reactivity (Fig. 6). The C=O group is observed as electrophilic.

NBO analysis

The natural bond orbitals (NBO) calculations were performed using NBO 3.1 program [51] as implemented in the Gaussian09 package at the DFT/B3LYP level in order to understand various second-order interactions between the filled orbitals of one subsystem and vacant orbitals of another subsystem, which is a measure of the intermolecular delocalization or hyper conjugation. NBO analysis provides the most accurate possible 'natural Lewis structure' picture of 'j' because all orbital details are mathematically chosen to include the highest possible percentage of the electron density. A useful aspect of the NBO method is that it gives information about interactions of both filled and virtual orbital spaces that could enhance the analysis of intra and inter molecular interactions. The second-order Fock-matrix was carried out to evaluate the donor–acceptor interactions in the NBO basis. The interactions result in a loss of occupancy from the localized NBO of the idealized Lewis structure into an empty non-Lewis orbital. For each donor (i) and acceptor (j) the stabilization energy ($E2$) associated with the delocalization $i \rightarrow j$ is determined as

$$E(2) = \Delta E_{ij} = q_i \frac{(F_{i,j})^2}{(E_j - E_i)}$$

q_i is donor orbital occupancy, E_i, E_j is the diagonal elements, and F_{ij} is the off diagonal NBO Fock matrix element.

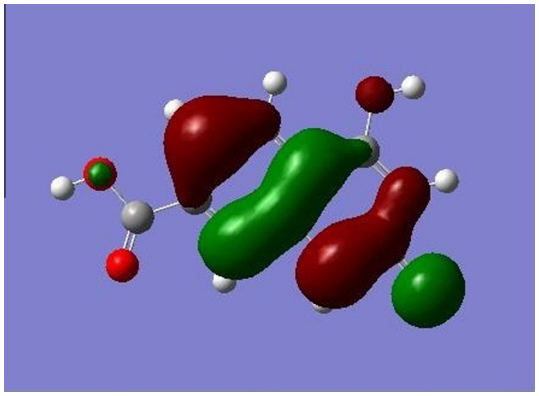

Fig. 4. HOMO plot of 4-hydroxy-2-oxo-1,2-dihydroquinoline-7-carboxylic acid.

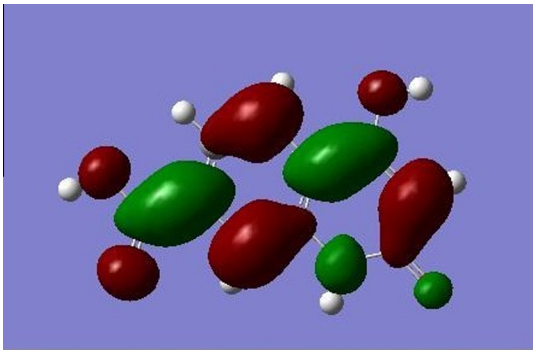

Fig. 5. LUMO plot of 4-hydroxy-2-oxo-1,2-dihydroquinoline-7-carboxylic acid.

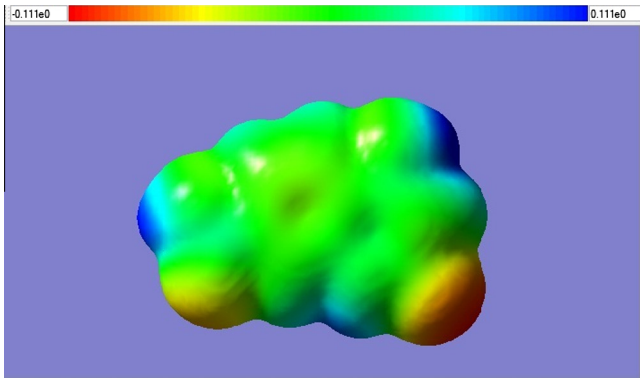

Fig. 6. MEP plot of 4-hydroxy-2-oxo-1,2-dihydroquinoline-7-carboxylic acid.

In NBO analysis large $E(2)$ value shows the intensive interaction between electron-donors and electron- acceptors, and greater the extent of conjugation of the whole system, the possible intensive interaction are given in Table 3. The second-order perturbation theory analysis of Fock-matrix in NBO basis shows strong intermolecular hyper conjugative interactions are formed by orbital overlap between n(O), n(N) and σ*(N—C), π*(C—C), σ*C—O, π*(C—O),bond orbitals which result in ICT causing stabilization of the system. These interactions are observed as an increase in electron density (ED) in N—C, C—O and C—C anti bonding orbital that weakens the respective bonds. There occurs a strong inter molecular hyper conjugative interaction of N_{14}—C_{20} from O_{22} of $n_2(O_{22}) \rightarrow \sigma^*(N_{14}$—$C_{20})$ which increases ED(0.08934e) that weakens the respective bonds N_{14}—C_{20} leading to stabilization of 29.22 kJ/mol and also the hyper conjugative interaction of C_{15}—C_{18} from O_{16} of $n_2(O_{16}) \rightarrow \pi^*(C_{15}$—$C_{18})$ which increases ED (0.24448e) that weakens the respective bonds C_{15}—C_{18} leading to stabilization of 33.85 kJ/mol. There occurs a strong inter molecular hyper conjugative interaction of C_{20}—O_{22} from N_{14} of $n_1(N_{14}) \rightarrow \pi^*(C_{20}$—$O_{22})$ which increases ED (0.3452e) that weakens the respective bonds C_{20}—O_{22} leading to stabilization of 52.08KJ/mol and also the hyper conjugative interaction of C_{10}—O_{11} from O_{12} of $n_2(O_{12}) \rightarrow \sigma^*(C_{10}$—$O_{11})$ which increases ED (0.09893e) that weakens the respective bonds C_{10}—O_{11} leading to stabilization of 34.4 kJ/mol. Again a hyper conjugative interaction of C_{10}—O_{12} from O_{11} of $n_2(O_{11}) \rightarrow \pi^*(C_{10}$—$O_{12})$ which increases ED (0.2263e) that weakens the respective bonds C_{10}—O_{12} leading to stabilization of 39.15 kJ/mol. These interactions are observed as an increase in electron density (ED) in N—C, C—C and C—O anti bonding orbitals that weakens the respective bonds.

The increased electron density at the oxygen atoms leads to the elongation of respective bond length and a lowering of the corresponding stretching wave number. The electron density (ED) is transferred from the n(O) to the anti-bonding π* orbital of the

Table 3
Second-order perturbation theory analysis of Fock matrix in NBO basis corresponding to the intra molecular bonds of the title compound.

Donor(i)	Type	ED/e	Acceptor(j)	Type	ED/e	$E(2)$[a]	$E(j)-E(i)$[b]	$F(i,j)$[c]
C1—C2	σ	1.97383	C1—C6	σ*	0.01922	2.83	1.29	0.054
–	σ	–	C2—C3	σ*	0.02917	3.94	1.25	0.063
–	σ	–	C3—C15	σ*	0.03427	2.49	1.2	0.049
–	σ	–	C6—C10	σ*	0.07512	2.62	1.12	0.049
–	σ	–	N14—C20	σ*	0.08934	2.82	1.14	0.051
C1—C6	σ	1.97106	C1—C2	σ*	0.01894	2.71	1.27	0.052
–	σ	–	C2—N14	σ*	0.02715	4.2	1.17	0.063
–	σ	–	C5—C6	σ*	0.02353	4.07	1.26	0.064
C1—C6	π	1.67932	C2—C3	π*	0.45361	20.96	0.28	0.07
–	π	–	C4—C5	π*	0.30278	17.31	0.29	0.063
–	π	–	C10—O12	π*	0.2263	16.52	0.3	0.064
C2—C3	σ	1.96497	C1—C2	σ*	0.01894	3.31	1.26	0.058
–	σ	–	C3—C4	σ*	0.01989	3.45	1.26	0.059
–	σ	–	C3—C15	σ*	0.03427	2.24	1.19	0.046
–	σ	–	N14—H21	σ*	0.0173	2.45	1.14	0.047
–	σ	–	C15—O16	σ*	0.02403	2.75	1.05	0.048
C2—C3	π	1.57665	C1—C6	π*	0.34743	17.19	0.29	0.064
–	π	–	C4—C5	π*	0.30278	21.01	0.29	0.071
–	π	–	C15—C18	π*	0.24448	17.43	0.29	0.066
C3—C4	σ	1.97292	C2—C3	σ*	0.02917	4.02	1.24	0.063
–	σ	–	C2—N14	σ*	0.02715	3.23	1.17	0.055
–	σ	–	C3—C15	σ*	0.03427	2.95	1.19	0.053
–	σ	–	C4—C5	σ*	0.0142	2.59	1.29	0.052
C3—C15	σ	1.96862	C1—C2	σ*	0.01894	2.68	1.25	0.052
–	σ	–	C3—C4	σ*	0.01989	3.07	1.25	0.055
–	σ	–	C15—C18	σ*	0.02142	3.05	1.3	0.056
C4—C5	σ	1.97872	C3—C4	σ*	0.01989	2.94	1.27	0.055
–	σ	–	C3—C15	σ*	0.03427	3.45	1.2	0.058
–	σ	–	C5—C6	σ*	0.02353	3.18	1.26	0.057
–	σ	–	C6—C10	σ*	0.07512	3.27	1.12	0.055
C4—C5	π	1.69747	C1—C6	π*	0.34743	20.77	0.29	0.07
–	π	–	C2—C3	π*	0.45361	16.4	0.28	0.063
C5—C6	σ	1.97594	C1—C6	σ*	0.01922	4.01	1.28	0.064
–	σ	–	C4—C5	σ*	0.0142	2.73	1.29	0.053
C6—C10	σ	1.98263	C1—C2	σ*	0.01894	2.91	1.23	0.053
–	σ	–	C4—C5	σ*	0.0142	2.09	1.25	0.046
C10—O12	π	1.98159	C1—C6	π*	0.34743	3.45	0.41	0.37
O11—H13	σ	1.98541	C10—O12	σ*	0.02288	5.2	1.36	0.075
N14—C20	σ	1.98864	C1—C2	σ*	0.01894	2.61	1.35	0.053
N14—H21	σ	1.98469	C2—C3	σ*	0.02917	4.05	1.2	0.062
–	σ	–	C18—C20	σ*	0.05679	3.06	1.14	0.053
–	σ	–	C20—O22	σ*	0.00876	0.6	1.27	0.025
C15—C18	σ	1.98256	C3—C4	σ*	0.01989	2.5	1.31	0.051
–	σ	–	C3—C15	σ*	0.03427	3.78	1.24	0.061
–	σ	–	C20—O22	σ*	0.00876	2.36	1.36	0.052
C15—C18	π	1.81263	C2—C3	π*	0.45361	9.95	0.3	0.052
–	π	–	C15—C18	π*	0.24448	2.04	0.31	0.023
–	π	–	C20—O22	π*	0.3452	22.91	0.31	0.078
O16—H17	σ	1.98824	C3—C15	σ*	0.03427	5.02	1.24	0.071
C18—C20	σ	1.97472	N14—H21	σ*	0.0173	2.57	1.11	0.048
–	σ	–	C15—O16	σ*	0.02403	5.34	1.02	0.066
–	σ	–	C15—C18	σ*	0.02403	2.52	1.28	0.051
C20—O22	σ	1.99488	C2—N14	σ*	0.02715	1.79	1.5	0.046
C20—O22	σ	–	C18—C20	σ*	0.05679	1.72	1.51	0.046
C20—O22	π	1.98133	C15—C18	π*	0.24448	5.05	0.37	0.041
C20—O22	π	–	C20—O22	π*	0.3452	1.22	0.37	0.021
LPO11	σ	1.97587	C6—C10	σ*	0.07512	5.86	1.00	0.069
–	σ	–	C10—O12	σ*	0.02288	1.23	1.2	0.034
LPO11	π	1.82419	C10—O12	σ*	0.02288	1.27	0.93	0.032
–	π	–	C10—O12	π*	0.2263	39.15	0.36	0.107
LPO12	σ	1.97824	C6—C10	σ*	0.07512	2.87	1.08	0.05
LPO12	π	1.84101	C6—C10	σ*	0.07512	19.53	0.65	0.103
–	π	–	C10—O11	σ*	0.09893	34.4	0.6	0.13
LPN14	σ	1.63393	C2—C3	π*	0.45361	46.39	0.28	0.103
–	σ	–	C20—O22	π*	0.3452	52.08	0.29	0.11
LPO16	σ	1.97788	C15—C18	σ*	0.02403	6.26	1.22	0.078
LPO16	π	1.85418	C15—C18	π*	0.24448	33.85	0.36	0.102
LPO22	σ	1.97692	C18—C20	σ*	0.05679	2.81	1.13	0.051
LPO22	π	1.85859	N14—C20	σ*	0.08934	29.22	0.65	0.125
LPO22	π	–	C18—C20	σ*	0.05679	18.99	0.7	0.105

[a] $E(2)$ means energy of hyperconjugative interactions (stabilization energy).
[b] Energy difference between donor and acceptor i and j NBO orbitals.
[c] $F(i,j)$ is the Fock matrix element between i and j NBO orbitals.

N—C, C—C and C—O bonds, explaining both the elongation and the red shift [52]. The hyper conjugative interaction energy was deduced from the second-order perturbation approach. Delocalization of electron density between occupied Lewis-type (bond or lone pair) NBO orbitals and formally unoccupied (anti bond or Rydberg) non-Lewis NBO orbitals corresponds to a stabilizing donor–acceptor interaction. The COOH, C=O and OH stretching modes can be used as a good probe for evaluating the bonding configuration around the atoms and the electronic distribution in the ring. Hence the structure 4-hydroxy-2-oxo-1, 2dihydroquinoline-7-carboxylic acid is stabilized by these orbital interactions.

The NBO analysis also describes the bonding in terms of the natural hybrid orbital $n_2(O_{11})$, which occupy a higher energy orbital (−0.33875a.u) with considerable p-character (99.62%) and low occupation number (1.82419) and the other $n_1(O_{11})$ occupy a lower energy orbital (−0.60542a.u.) with p-character (55.88%) and high occupation number (1.97587).The NBO analysis also describes the bonding in terms of the natural hybrid orbital $n_2(O_{12})$, which occupy a higher energy orbital (−0.25807 a.u) with considerable p-character (99.68%) and low occupation number (1.84101) and the other $n_1(O_{12})$ occupy a lower energy orbital (−0.68592 a.u) with p-character (41.90%) and high occupation number (1.97824).The NBO analysis also describes the bonding in terms of the natural hybrid orbital $n_2(O_{16})$, which occupy a higher energy orbital (−0.34868 a.u) with considerable p-character (99.88%) and low occupation number (1.85418) and the other $n_1(O_{16})$ occupy a lower energy orbital (−0.62307a.u) with p-character (55.87%) and high occupation number (1.9778). The NBO analysis also describes the bonding in terms of the natural hybrid orbital $n_2(O_{22})$, which occupy a higher energy orbital (−0.23775 a.u) with considerable p-character (99.76%) and low occupation number (1.85859) and the other $n_1(O_{22})$ occupy a lower energy orbital(−0.66943a.u) with p-character (40.70%) and high occupation number (1.97692). Thus, a very close to pure p-type lone pair orbital participates in the electron donation to the $\sigma^*(N_{14}—C_{20})$ orbital for $n_2(O_{22}) \rightarrow \sigma^*(N_{14}—C_{20})$, $\pi^*(C_{15}—C_{18})$ orbital for $n_2(O_{16}) \rightarrow \pi^*(C_{15}—C_{18})$, $\pi^*(C_{10}—O_{11})$ orbital for $n_2(O_{12}) \rightarrow \pi^*(C_{10}—O_{11})$ and $\pi^*(C_{10}—O_{12})$ orbital for $n_2(O_{11}) \rightarrow \pi^*(C_{10}—O_{12})$ interaction in the compound. The results are tabulated in Table 4.

First hyperpolarizability

Nonlinear optics deals with the interaction of applied electromagnetic fields in various materials to generate new electromagnetic fields, altered in wavenumber, phase, or other physical properties [53]. Organic molecules able to manipulate photonic signals efficiently are of importance in technologies such as optical communication, optical computing, and dynamic image processing [54,55]. In this context, the dynamic first hyperpolarizability of the title compound is also calculated in the present study. The first hyperpolarizability (β_0) of this novel molecular system is calculated using SDD method, based on the finite field approach. In the presence of an applied electric field, the energy of a system is a function of the electric field. First hyperpolarizability is a third rank tensor that can be described by a $3 \times 3 \times 3$ matrix. The 27 components of the 3D matrix can be reduced to 10 components due to the Kleinman symmetry [56]. The components of β are defined as the coefficients in the Taylor series expansion of the energy in the external electric field. When the electric field is weak and homogeneous, this expansion becomes

$$E = E_0 - \sum_i \mu_i F^i - \frac{1}{2}\sum_{ij} \alpha_{ij} F^i F^j - \frac{1}{6}\sum_{ijk} \beta_{ijk} F^i F^j F^k - \frac{1}{24}\sum_{ijkl} \gamma_{ijkl} F^i F^j F^k F^l + \ldots$$

where E_0 is the energy of the unperturbed molecule, F^i is the field at the origin, μ_{ij}, α_{ij}, β_{ijk} and γ_{ijkl} are the components of dipole moment, polarizability, the first hyperpolarizabilities, and second hyperpolarizabilities, respectively. The calculated first hyperpolarizability of the title compound is 6.37×10^{-30} e.s.u which is 49 times that of standard NLO material urea (0.13×10^{-30} e.s.u) [57]. The reported values of hyperpolarizability of similar derivatives are 2.24×10^{-30} e.s.u [58] and 2.24×10^{-30} e.s.u [59].

Table 4
NBO results showing the formation of Lewis and non-Lewis orbitals.

Bond(A-B)	ED/ energy	EDA%	EDB%	NBO	s%	p%
σC1—C2	1.97383	48.56	51.44	$0.6968(sp^{1.91})C$	34.45	65.61
–	−0.72557	–	–	$+0.7172(sp^{1.72})C$	36.71	63.26
σC1—C6	1.97106	49.16	50.84	$0.7011(sp^{1.83})C$	35.35	64.61
–	−0.72045	–	–	$+0.7131(sp^{1.86})C$	35.01	64.95
πC1—C6	1.67932	49.30	50.70	$0.7022(sp^{1.00})C$	0.00	99.95
–	−0.27495	–	–	$+0.7120(sp^{1.00})C$	0.00	99.97
σC2—C3	1.96497	49.89	50.11	$0.7063(sp^{1.87})C+$	34.86	65.10
–	−0.71500	–	–	$0.7079(sp^{2.07})C$	32.54	67.41
πC2—C3	1.57665	45.48	54.52	$0.6744(sp^{1.00})C+$	0.00	99.97
–	−0.27424	–	–	$0.7383(sp^{1.00})C$	0.00	99.98
σC3—C4	1.97292	51.76	48.24	$0.7194(sp^{1.82})C+$	35.47	64.50
–	−0.71429	–	–	$0.6946(sp^{1.94})C$	33.98	65.98
σC3—C15	1.96862	51.04	48.96	$0.7144(sp^{2.13})C+$	31.93	68.04
–	−0.70201	–	–	$0.6997(sp^{1.89})C$	34.57	65.39
σC4—C5	1.97872	49.85	50.15	$0.7061(sp^{1.79})C+$	35.87	64.09
–	−0.72316	–	–	$0.7081(sp^{1.78})C$	35.96	64.01
πC4—C5	1.69747	47.31	52.69	$0.6878(sp^{1.00})C+$	0.00	99.95
–	−0.27580	–	–	$0.7259(sp^{1.00})C$	0.00	99.96
σC5—C6	1.97594	48.98	51.02	$0.6999(sp^{1.91})C+$	34.38	65.58
–	−0.71772	–	–	$0.7143(sp^{1.83})C$	35.29	64.68
σC6—C10	1.98263	53.13	46.87	$0.7289(sp^{2.37})C+$	29.68	70.27
–	−0.68235	–	–	$0.6846(sp^{1.58})C$	38.77	61.17
πC10—O12	1.98159	31.84	68.16	$0.5643(sp^{99.99})C+$	0.87	98.95
–	−0.40078	–	–	$0.8256(sp^{97.97})O$	1.01	98.65
πO11—H13	1.98541	74.95	25.05	$0.8657(sp^{3.51})O+$	22.13	77.77
–	−0.76561	–	–	$0.5005(sp)H$	100.0	0.00
σN14—C20	1.98864	63.82	36.18	$0.7989(sp^{1.81})N+$	35.52	64.46
–	−0.80909	–	–	$0.6015(sp^{2.47})C$	28.80	71.06
σN14—H21	1.98469	72.44	27.56	$0.8511(sp^{2.71})N+$	26.96	73.00
–	−0.67372	–	–	$0.5250(sp)H$	100.0	0.00
σC15—C18	1.98256	50.68	49.32	$0.7119(sp^{1.48})C+$	40.34	59.62
–	−0.76385	–	–	$0.7023(sp^{1.73})C$	36.59	63.37
σO16—H17	1.98824	75.24	24.76	$0.8674(sp^{3.79})O+$	20.86	79.04
–	−0.76472	–	–	$0.4976(sp)H$	100.0	0.00
σC18—C20	1.97472	51.53	48.47	$0.7178(sp^{2.03})C+$	33.00	66.95
–	−0.68790	–	–	$0.6962(sp^{1.66})C$	37.61	62.34
σC20—O22	1.99488	35.50	64.50	$0.5958(sp^{1.99})C+$	33.37	66.55
–	−1.04684	–	–	$0.8031(sp^{1.45})O$	40.70	58.95
πC20—O22	1.98133	30.48	69.52	$0.5520(sp^{1.00})C+$	0.00	99.82
–	−0.35729	–	–	$0.8338(sp^{1.00})O$	0.00	99.69
n1O11	1.97587	–	–	$sp^{1.27}$	44.05	55.88
–	−0.60542	–	–	–	–	–
n2O11	1.82419	–	–	$sp^{99.99}$	0.24	99.62
–	−0.33875	–	–	–	–	–
n1O12	1.97824	–	–	$sp^{0.72}$	58.05	41.90
–	−0.68592	–	–	–	–	–
n2O12	1.84101	–	–	$sp^{99.99}$	0.05	99.68
–	−0.25807	–	–	–	–	–
n1N14	1.63393	–	–	$sp^{1.00}$	0.00	99.99
–	−0.27299	–	–	–	–	–
n1O16	1.97788	–	–	$sp^{1.27}$	44.07	55.87
–	−0.62307	–	–	–	–	–
n2O16	1.85418	–	–	$sp^{1.00}$	0.00	99.88
–	−0.34868	–	–	–	–	–
n1O22	1.97692	–	–	$sp^{0.69}$	59.26	40.70
–	−0.66943	–	–	–	–	–
n2O22	1.85859	–	–	$sp^{1.00}$	0.00	99.76
–	−0.23775	–	–	–	–	–

Mulliken charges

The calculation of atomic charges plays an important role in the application of quantum mechanical calculations to molecular systems. Mulliken charges are calculated by determining the electron population of each atom as defined in the basis functions. The

Table 5
The charge distribution calculated by the Mulliken and natural bond orbital (NBO) methods.

Atoms	Natural charges	Atomic charges (Mulliken)
C1	−0.21736	−0.219867
C2	0.20592	0.373073
C3	−0.12858	0.077297
C4	−0.18207	−0.190057
C5	−0.25467	−0.208148
C6	−0.15446	0.055495
H7	0.26311	0.173589
H8	0.26071	0.168935
H9	0.23493	0.138573
C10	0.81533	0.556073
O11	−0.69270	−0.572463
O12	−0.56481	−0.441284
H13	0.49212	0.413611
N14	−0.60169	−0.773521
C15	0.38035	0.388914
O16	−0.67692	−0.630725
H17	0.50016	0.423126
C18	−0.40307	−0.321182
H19	0.25157	0.145938
C20	0.64612	0.629530
H21	0.43716	0.341485
O22	−0.61115	−0.528390

charge distributions calculated by the Mulliken [60] and NBO methods for the equilibrium geometry of 4-hydroxy-2-oxo-1,2-dihydroquinoline-7-carboxylic acid are given in Table 5. The charge distribution on the molecule has an important influence on the vibrational spectra. In 4-hydroxy-2-oxo-1,2-dihydroquinoline-7-carboxylic acid, the distribution of Mulliken atomic charge shows the direction of delocalization and shows that the natural atomic charges are more sensitive to the changes in the molecular structure than Mulliken's net charges. Also we have done a comparison of Mulliken charges obtained by different basic sets and tabulated it in Table 6 in order to assess the sensitivity of the calculated charges to changes in (i) the choice of the basis set; (ii) the choice of the quantum mechanical method. The results can, however, better be represented in graphical form as shown in Fig. 7. We have observed a change in the charge distribution by changing different basis sets.

Table 6
Calculated Mulliken charges of 4-hydroxy-2-oxo-1,2-dihydroquinoline-7-carboxylic acid.

Atom	HF/6-31G*	B3LYP/6-31G*	B3LYP/SDD
1C	−0.161892	−0.217144	−0.551223
2C	0.418438	0.363171	0.313182
3C	−0.128283	0.081031	0.203842
4C	−0.166426	−0.188513	−0.351728
5C	−0.211630	−0.197606	−0.352503
6C	−0.149026	0.064790	0.274918
7H	0.306366	0.170256	0.278391
8H	0.285998	0.165798	0.272969
9H	0.212973	0.133730	0.218891
10C	0.832058	0.551207	0.197455
11O	−0.702959	−0.578846	−0.395868
12O	−0.593946	−0.438970	−0.229133
13H	0.440674	0.416503	0.367378
14N	−1.045790	−0.764426	−0.425281
15C	0.500846	0.399033	0.297518
16O	−0.757717	−0.641619	−0.443676
17H	0.446217	0.423398	0.379367
18C	−0.329380	−0.315705	−0.472343
19H	0.231776	0.145655	0.237961
20C	0.823594	0.628370	0.100899
21H	0.405187	0.338624	0.340148
22O	−0.657079	−0.538737	−0.261164

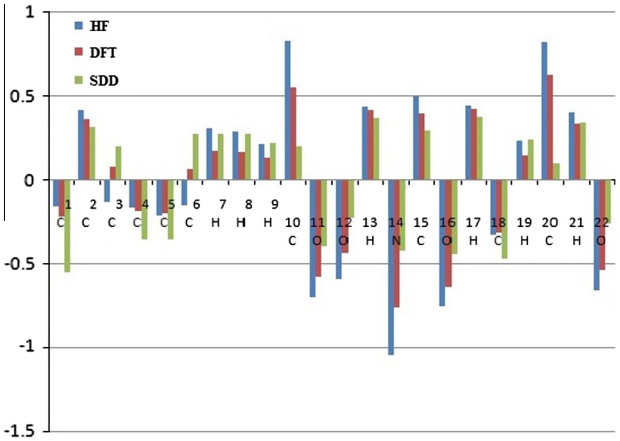

Fig. 7. Comparison of different methods for calculated Mulliken charges of 4-hydroxy-2-oxo-1,2-dihydroquinoline-7-carboxylic acid.

PES scan studies

A detailed potential energy surface (PES) scan on dihedral angles C_{10}—C_6—C_1—C_2 and O_{11}—C_{10}—C_6—C_1 have been performed at B3LYP/6-31G(d) level to reveal all possible conformations of 4-hydroxy-2-oxo-1,2-dihydroquinoline-7-carboxylic acid. The PES scan was carried out by minimizing the potential energy in all geometrical parameters by changing the torsion angle at every 10° for 180° rotation around the bond. The results obtained in PES scan study by varying the torsion perturbation around C═O are plotted in Figs. 8 and 9. For the C_{10}—C_6—C_1—C_2 rotation, the minimum energy was obtained at −179.0° in the potential energy curve of energy −740.7352 Hartrees. For the O_{11}—C_{10}—C_6—C_1 rotation, the minimum energy occurs at −19.9° in the potential energy curve of energy −740.8471 Hartrees.

^{1}H NMR spectrum

With TMS as internal standard, experimental spectrum data of 4-hydroxy-2-oxo-1,2 dihydroquinoline-7-carboxylic acid in DMSO is obtained at 500 MHz and is shown in Table 7. B3LYP/GIAO was used to calculate the absolute isotropic chemical shielding of 4-hydroxy-2-oxo-1,2-dihydroquinoline-7-carboxylic acid [61]. Relative chemical shifts were then estimated by using the corresponding TMS shielding: σ_{calc}(TMS) calculated in advance at the same theoretical level as this paper. Numerical values of chemical shift

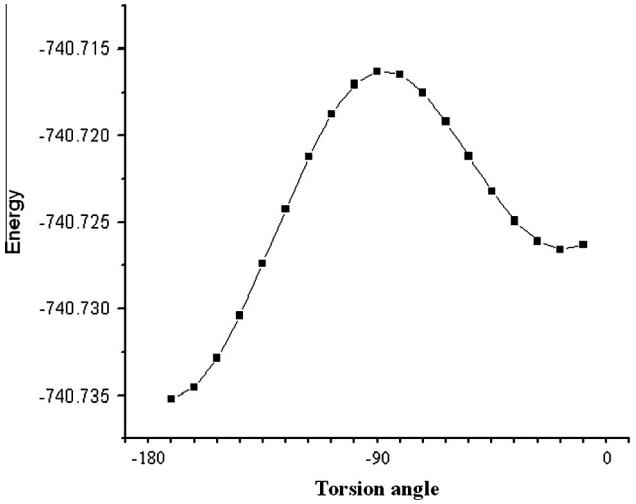

Fig. 8. Profile of potential energy scan for the torsion angle C10—C6—C1—C2.

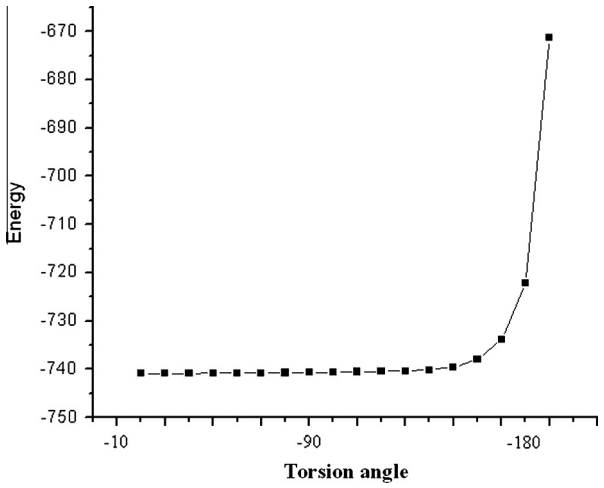

Fig. 9. Profile of potential energy scan for the torsion angle O11—C10—C6—C1.

Table 7
Experimental and calculated ^{1}H NMR parameters (with respect to TMS).

Protons	σ_{TMS}	B3LYP/6-31G	$\delta_{calc} = \sigma_{TMS} - \sigma_{calc}$	Exp δ_{ppm}
H7	32.7711	24.8333	7.9378	8.03
H8		24.3405	8.4306	8.2
H9		25.2337	7.5374	8.2
H13		24.0689	6.7022	5.9
H17		26.2989	6.4722	5.9
H19		26.7591	6.0120	5.6
H21		24.9210	7.8501	7.8

$\delta_{pred} = \sigma_{calc}(TMS) - \sigma_{calc}$ together with calculated values of σ_{calc} (TMS), are reported in Table 7. It is seen that chemical shift was in agreement with the experimental ^{1}H NMR data. Thus, the results has shown that the predicted proton chemical shifts were in good agreement with the experimental data for 4-hydroxy-2-oxo-1,2-dihydroquinoline-7-carboxylic acid.

Conclusion

The vibrational spectroscopic studies of 4-hydroxy-2-oxo-1,2-dihydroquinoline-7-carboxylic acid in the ground state were reported experimentally and theoretically. Potential energy distribution of normal modes of vibrations was done using GAR2PED program. The ring stretching modes in IR and Raman spectra are evidence for charge transfer interaction between the donor and the acceptor group through the π system. This along with the lowering of HOMO–LUMO band gap supports for the bioactivity of the molecule. NBO analysis predicts a strong inter molecular hyper conjugative interaction of (N_{14}—C_{20}) from O_{22} of $n_2(O_{22})$, (C_{15}—C_{18}) fromO_{16} of $n_2(O_{16})$ (C_{10}—O_{11}) from O_{12} of $n_2(O_{12})$ and (C_{10}—O_{12}) from O_{11} of $n_2(O_{11})$. MEP predicts the most reactive part in the molecule. The calculated first hyperpolarizability is comparable with the reported values of similar derivatives and is an attractive object for future studies in nonlinear optics. The minimum energy surfaces are obtained from the potential energy curve by PES scan studies. In addition the calculated ^{1}H NMR results are in good agreement with experimental data.

Acknowledgements

The authors are thankful to University of Antwerp for access to the university's CalcUA Supercomputer Cluster. RTU thanks University of Kerala for a research fellowship.

References

[1] A.G. Mac Diarmid, A.J. Epstein, in: S.A. Jenekhe, K.J. Wynne (Eds.), Photonic and Optoelectronic Polymers, American Chemical Society, Washington, DC, 1997, p. 395.
[2] A.J. Epstein, Mater. Res. Soc. Bull. 22 (1997) 16–24.
[3] S. Yamaguchi, M. Goto, H. Takayanagi, H. Ogura, Bull. Chem. Soc. Jpn. 61 (1988) 1026–1028.
[4] P. Zaderenko, M.S. Gel, P. Lopez, P. Ballesteros, I. Fonseco, A. Albert, Acta Cryst. B53 (1997) 961–967.
[5] M.L. Martinez, W.C. Cooper, P.T. Chou, Chem. Phys. Lett. 193 (1992) 151–154.
[6] E.L. Roberts, P.T. Chou, T.A. Alexander, R.A. Agbaria, I.M. Warner, J. Phys. Chem. 99 (1995) 5431–5437.
[7] A.I. Sytnik, J.C. Del Valle, J. Phys. Chem. 99 (1995) 13028–13032.
[8] M. Kubicki, T. Borowiak, W.Z. Antkowiak, Acta Cryst. C: Cryst. Struct. Commun. 51 (1995) 1173–1175.
[9] P.T. Chou, C.Y. Wei, J. Phys. Chem. 100 (1996) 17059–17066.
[10] D. LeGourrierec, V. Kharlanov, R.G. Brown, W. Rettig, J. Photochem. Photobiol. A: Chem. 117 (1998) 209–216.
[11] P.T. Chou, C.Y. Wei, W.S. Yu, Y.H. Chou, J. Phys. Chem. A 105 (2001) 1731–1740.
[12] X.S. Wu, H.S. Sun, Y. Pan, H.B. Chen, X.Z. Sun, Chin. Chem. Lett. 10 (1999) 875–878.
[13] H. Matsumiya, H. Hoshino, T. Yotsuyanagi, Analyst 126 (2001) 2082–2086.
[14] P.T. Chou, G.R. Wu, Y.I. Liu, W.S. Yu, J. Phys. Chem. A 106 (2002) 5967–5973.
[15] H. Matsumiya, H. Hoshino, Anal. Chem. 75 (2003) 413–419.
[16] S. Takeuchi, T. Tahara, J. Phys. Chem. A 109 (2005) 10199–10207.
[17] C.H. Chen, J.M. Shi, Coord. Chem. Rev. 171 (1998) 161–174.
[18] A.P. Kulkarni, C.J. Tonzola, A. Babel, S.A. Jenekhe, Chem. Mater. 16 (2004) 4556–4573.
[19] J. Dancey, E.A. Elsenhauer, Br. J. Cancer 74 (1996) 327–338.
[20] M. Potmesil, H.M. Pinedo, Camptothecins: New Anticancer Agents, CRC Press, Boca, Raton, 1995.
[21] C.H. Takimoto, J. Wrigth, S.G. Arbuck, Biochim. Biophys. Acta 1400 (1998) 107–119.
[22] R.E. Bambury, in: M.E. Wolff (Ed.), Burger's Medicinal Chemistry, Part II, John Wiley, New York, 1979, pp. 41–81.
[23] K. Tsushima, T. Osumi, N. Matsuo, N. Itaya, Agric. Biol. Chem. 53 (1989) 2529–2530.
[24] J. Jampilek, R. Musiol, M. Pesko, K. Kralova, M. Vejsova, J. Carroll, A. Coffey, J. Finster, D. Tabak, H. Niedbala, V. Kozik, J. Polanski, J. Csollei, J. Dohnal, Molecules 14 (2009) 1145–1159.
[25] M.J. Frisch, G.W. Trucks, H.B. Schlegel, G.E. Scuseria, M.A. Robb, J.R. Cheeseman, G. Scalmani, V. Barone, B. Mennucci, G.A. Petersson, H. Nakatsuji, M. Caricato, X. Li, H.P. Hratchian, A.F. Izmaylov, J. Bloino, G. Zheng, J.L. Sonnenberg, M. Hada, M. Ehara, K. Toyota, R. Fukuda, J. Hasegawa, M. Ishida, T. Nakajima, Y. Honda, O. Kitao, H. Nakai, T. Vreven, J.A. Montgomery, Jr., J. E. Peralta, F. Ogliaro, M. Bearpark, J.J. Heyd, E. Brothers, K.N. Kudin, V.N. Staroverov, T. Keith, R. Kobayashi, J. Normand, K. Raghavachari, A. Rendell, J.C. Burant, S.S. Iyengar, J. Tomasi, M. Cossi, N. Rega, J.M. Millam, M. Klene, J.E. Knox, J.B. Cross, V. Bakken, C. Adamo, J. Jaramillo, R. Gomperts, R.E. Stratmann, O. Yazyev, A.J. Austin, R. Cammi, C. Pomelli, J.W. Ochterski, R.L. Martin, K. Morokuma, V.G. Zakrzewski, G. A. Voth, P. Salvador, J.J. Dannenberg, S. Dapprich, A.D. Daniels, O. Farkas, J.B. Foresman, J.V. Ortiz, J. Cioslowski, D.J. Fox, Gaussian Inc., Wallingford CT, Gaussian 09, Revision B.01, 2010.
[26] J.B. Foresman, in: E. Frisch (Ed.), Exploring Chemistry with Electronic Structure Methods: A Guide to Using Gaussian, Gaussian Inc., Pittsburg, PA, 1996.
[27] P.J. Hay, W.R. Wadt, J. Chem. Phys. 82 (1985) 270–283.
[28] J. Zhao, Y. Zhang, L. Zhu, J. Mol. Struct. Theochem. 671 (2004) 179–187.
[29] R. Dennington, T. Keith, J. Millam, Semichem Inc., Shawnee Mission KS, GaussView, Version 5, 2009.
[30] J.M.L. Martin, C. Van Alsenoy, GAR2PED, A Program to Obtain a Potential Energy Distribution from a Gaussian Archive Record, University of Antwerp, Belgium, 2007.
[31] L.J. Bellamy, The IR Spectra of Complex Molecules, John Wiley & sons, New York, 1975.
[32] A. Spire, M. Barthes, H. Kallouai, G. De Nunzio, Physics D 137 (2000) 392–396.
[33] G. Socrates, Infrared Characteristic Group Frequencies, John Wiley and Sons, New York, 1981.
[34] N.P.G. Roeges, A Guide to the Complete Interpretation of IR Spectra of Organic Compounds, Wiley, New York, 1994.
[35] R. Minitha, Y.S. Mary, H.T. Varghese, C.Y. Panicker, R. Ravindran, K. Raju, V.M. Nair, J. Mol. Struct. 985 (2011) 316–322.
[36] C.Y. Panicker, H.T. Varghese, V.S. Madhavan, S. Mathew, J. Vinsova, C. Van Alsenoy, Y.S. Mary, Y.S. Mary, J. Raman Spectrosc. 40 (2009) 2176–2186.
[37] S. Kundoo, A.N. Banerjee, P. Saha, K.K. Chattophyay, Mater. Lett. 57 (2003) 2193–2197.
[38] H.T. Varghese, C.Y. Panicker, D. Philip, J. Chowdhury, M. Ghosh, J. Raman, Spectroscopy 38 (2007) 323–331.
[39] N.B. Colthup, L.H. Daly, S.E. Wiberly, Introduction to IR and Raman Spectroscopy, Academic Press, NewYork, 1990.
[40] G. Varsanyi, Assignments of Vibrational Spectra of Seven Hundred Benzene Derivatives, Wiley, New York, 1974.
[41] R.M. Silverstein, F.X. Webster, Spectrometric Identification of Organic Compounds, sixth ed., John Wiley, Asia, 2003.

[42] A.S. El-Shahway, S.M. Ahmed, N.K. Sayed, Spectrochim. Acta 66A (2007) 143–153.
[43] Y.S. Mary, H.T. Varghese, C.Y. Panicker, T. Ertan, I. Yildiz, O. Temiz-Arpaci, Spectrochim. Acta 71 (2008) 566–571.
[44] J. Chowdhury, M. Ghosh, T.N. Misra, Spectrochim. Acta 56 (2000) 2107–2115.
[45] V. Krishnakumar, N. Prabavathi, S. Muthunatesan, Spectrochim. Acta 69 (2008) 853–859.
[46] S. Yurdakul, M. Yurdakul, J. Mol. Struct. 834–836 (2007) 555–560.
[47] E. Scrocco, J. Tomasi, Adv. Quantum. Chem. 103 (1978) 115–193.
[48] F.J. Luque, J.M. Lopez, M. Orozco, Theor. Chem. Acc. 103 (2000) 343–345.
[49] P. Politzer, J.S. Murray, in: D.L. Beve ridge, R. Lavery, (Eds.), Theoretical Biochemistry and Molecular Biophysics, Springer, Berlin, 1991 (Chapter 13).
[50] E. Scrocco, J. Tomasi, Top. Curr. Chem. 42 (1973) 95–170.
[51] E.D. Glendening, A.E. Reed, J.E. Carpenter, F. Weinhold, NBO Version 3.1.
[52] J. Choo, S. Kim, H. Joo, Y. Kwon, J. Mol. Struct. (Theochem.) 587 (2002) 1–8.
[53] Y.R. Shen, The Principles of Nonlinear Optics, Wiley, New York, 1984.
[54] P.V. Kolinsky, Opt. Eng. 31 (1992) 1676–1684.
[55] D.F. Eaton, Science 25 (1991) 281–287.
[56] D.A. Kleinman, Phys. Rev. 126 (1962) 1977–1979.
[57] M. Adant, M. Dupuis, J.L. Bredas, Int. J. Quantum. Chem. 56 (1995) 497–507.
[58] G. Purohit, G.C. Joshi, Indian J. Pure Appl. Phys. 41 (2003) 922–927.
[59] A.J. Camargo, H.B. Napolitano, J. Zukerman-Schpector, J. Mol. Struct. (Theochem.) 816 (2007) 145–151.
[60] R.S. Mulliken, J. Chem. Phys. 23 (1955) 1833–1840.
[61] K. Wolinski, J.F. Hinton, P. Pulay, J. Am. Chem. Soc. 112 (1990) 8251–8260.